Applied Catalysis B: Environmental 226 (2018) 202–212

Contents lists available at ScienceDirect

Applied Catalysis B: Environmental

journal homepage: www.elsevier.com/locate/apcatb

Silver-modified manganite and ferrite perovskites for catalyzed gasoline particulate filters

Willinton Y. Hernández, Diego Lopez-Gonzalez, S. Ntais, C. Zhao, A. Boréave, Philippe Vernoux*

Université de Lyon, Institut de Recherches sur la Catalyse et l'Environnement de Lyon, UMR 5256, CNRS, Université Claude Bernard Lyon 1, 2 avenue A. Einstein, F-69626 Villeurbanne, France

ARTICLE INFO

Keywords:
Gasoline particulate filter
Perovskite
Silver
Soot combustion

ABSTRACT

Silver modified manganite (LaSrAgMn) and ferrite (LaSrAgFe) perovskites were synthesized with different Ag loadings and tested for the soot oxidation reaction at low oxygen concentrations (i.e. 1 vol%), as encountered in gasoline direct injection (GDI) engines application. The state and location of Ag determine the catalytic performances of perovskites. On ferrites, Ag is either partially incorporated on the structure or present on the surface as large agglomerates. Lattice Ag^{+} cations are not catalytically active. Furthermore, large surface Ag particles partially cover surface oxygen vacancies and block their ability to adsorb oxygen. On the other hand, small clusters of Ag and AgO as well as a surface $Ag_{1.8}Mn_8O_{16}$ additional hollandite-type phase are stabilized on manganites surface, improving the reducibility and acting as active sites for soot oxidation.

1. Introduction

Nowadays, there is a global consensus concerning the toxicity of fine particulate matter emissions (PM) from internal combustion engines. The contribution of the transport sector to PM2.5 (Particulates smaller than 2.5 μm) emissions is around 14% in Europe. To still reduce this impact, the recent Euro 6c European legislations implemented from September 2017 for new passenger cars have strengthened the emissions limits of Particulates Number (PN) of Gasoline Direct Injection (GDI) vehicles to reach the level of Diesel cars, i.e. 6.0×10^{11} particulates/km. Due to their improved fuel efficiency [1], an increase in European and US market penetration of GDI vehicles is expected in a near future.

A first approach to tackle PM emissions is to incorporate a particulate filter downstream the three-way converter (TWC) in the exhaust of GDI engines, as for Diesel cars. Although gasoline particulate filters (GPF) are being considered as a plausible solution due to their great success in Diesel engine; the growing back pressure generated by soot cake formation could seriously penalize the efficiency of this type of engines [2]. To overcome this drawback, the filter has to be periodically regenerated in an efficient manner. However, the low amount of oxygen downstream the TWC as well as the high temperatures required for oxidizing soot (≈600 °C) restrict the possible regeneration strategies [3]. In this regard, most efforts are led to the development of an effective catalytic formulation to oxidize soot with oxygen at low oxygen partial pressures and temperature. To the best of our knowledge, the soot oxidation reaction in GDI exhaust conditions has been hardly reported in literature (i.e. ≤10.000 ppm of O_2).

Different types of catalysts have been proposed as an effective solution for soot oxidation with oxygen such ceria [4,5], alkali-based oxides [6], Yttria-Stabilized Zirconia (YSZ) [7,8] or perovskites [13],9]. This latter family of oxides are very attractive since their formulation can be adapted to tailor the catalytic oxidation activity [10]. Perovskites are mixed oxides with a general formula ABO_3 being the A-cation larger than the B-one. The versatility of these materials lies on the fact that around 90% of the metallic natural elements of the periodic table are known to be stable in a perovskite type oxide structure [10]. Moreover, multicomponent perovskites synthesis is possible by partial substitution of cations in positions A and B, giving rise to substituted compounds with formula $A_{1-x}A'_xB_{1-x}B'_xO_3$. The substitution of A and/or B atoms with metals with different oxidation degrees may enhance the catalytic activity due to the formation of structural defects such as cationic or anionic vacancies and/or change the oxidation state of the transition metal to maintain the electroneutrality of the compound [11]. Then, the nature of the B cation determines the generation of new lattice defects, mixed valence states and non-stoichiometric oxygen [12]. Furthermore, the partial substitution of the A cation also influences the overall catalytic activity by affecting the oxidation state of the B site cation and the overall redox properties of the perovskite phase [13].

Our group has recently shown [3] that manganite and ferrite oxides ($La_{0.6}Sr_{0.4}BO_3$ with B = Fe or Mn) are efficient to oxide soot even at low

* Corresponding author.
E-mail address: philippe.vernoux@ircelyon.univ-lyon1.fr (P. Vernoux).

https://doi.org/10.1016/j.apcatb.2017.12.029
Received 15 September 2017; Received in revised form 24 November 2017; Accepted 11 December 2017
Available online 15 December 2017

oxygen partial pressures, which makes them especially suitable for GDI engines application. Nevertheless, the catalytic performances of these oxides have to be improved for a practical application. This study explores the impact of their partial substitution by Ag cations. Silver modified perovskites have been reported in the literature for catalytic diesel soot combustion [14–16] under excess of oxygen. Enhanced catalytic activity of Ag-modified perovskites was linked to improved redox properties due to presence of surface Ag nanoparticles (NPs). These latter are capable of activating oxygen by dissociative adsorption at low temperature [17] and supported Ag (NPs) are known to exhibit high catalytic activity towards soot oxidation in Diesel exhaust conditions, i.e. excess of oxygen [18–25].

In this study, a wide range of Ag-substituted lanthanum manganites (LaSrxAgMn) and ferrites (LaSrxAgFe) were prepared and their catalytic performances were investigated, for the first time, for the soot oxidation reaction under GDI engines conditions, i.e. low O_2 partial pressure. Perovskites were synthesized by a complex route involving the thermal decomposition of nitrates precursors. Physico-chemical properties of prepared perovskites as well as morphology and microstructure were assessed by means of X-Ray diffraction (XRD), X-Ray photoelectron spectroscopy (XPS), nitrogen adsorption-desorption isotherms, temperature programmed reduction (TPR), temperature programmed desorption (TPD), scanning electronic microscopy (SEM) and transmission electronic microscopy (TEM). The catalytic activity towards soot oxidation has been tested at low oxygen partial pressures, i.e. 1 vol.%.

2. Experimental

2.1. Perovskites synthesis

Perovskites were prepared by a complex route method from the thermal decomposition of the chelated nitrate precursor, as described elsewhere [26,27]. The nitrate precursors, including $AgNO_3$ (Sigma-Aldrich®, ≥99.0%), were dissolved in a 10% w/w aqueous solution of maleic acid (Alfa Aesar®, 99%). The molar ratios of La/Sr/Ag/(Mn or Fe)/maleic acid were employed as 0.5/0.5-x/x/1/8.6, varying the silver content (x) from 5 to 25% molar ratio with respect to the total A-site ions (La + Sr + Ag). After the dissolution of the salts, the pH of the mixture was fixed at 8 by adding ammonium hydroxide solution (Sigma-Aldrich®, 25% NH_3). Most of the water was then evaporated on a heating plate. The mixture was put overnight in an oven at 110 °C and produced a powder precursor. This last was heated at 350 °C (2 °C/min) for 2 h to remove the organic compounds and finally calcined at 800 °C (4 °C/min) for 4 h, under air flow. The obtained samples were named as LaSrxAgMn or LaSrxAgFe, according to the silver percentage introduced during the preparation and the chemical nature of the perovskites (M for manganites and F for ferrites).

2.2. Characterizations

The chemical composition of the samples was measured by inductively coupled plasma-emission spectroscopy, ICP-OES (Varian). Specific surface areas (SSA) were estimated according to the BET method by nitrogen adsorption at liquid nitrogen temperature in a Micromeritics ASAP 2000 apparatus. The samples were degassed 2 h at 300 °C under vacuum before measurements. The X-ray diffraction pattern of the materials was recorded at room temperature using X-ray power diffractometer Bruker D5005 with CuKα radiation (λ = 0.154178 nm) in a wide range of Bragg angles 2θ (20–80°) at a scanning rate of 5°/min. The microstructure and surface morphology were characterized with a scanning electron microscope (FEI ESEM-XL30) and a transmission electron microscope (TEM, JEOL 2010 LaB6). Catalysts were dispersed in ethanol and deposited on carbon grids. The weight-average silver crystallite size was calculated by measuring Ag nanoparticles with the ImageJ 1.44 software from at least 20 micrographs and over 100 nanoparticles.

Temperature-programmed desorption of oxygen (O_2-TPD) experiments were performed on a homemade instrument connected to a HPR-20 QIC HIDEN ANALYTICAL mass spectrometer, operated in selected ion mode with a SEM detector. 100 mg of catalyst sample were loaded in a fixed-bed tubular quartz reactor. After evacuation of the catalyst at 500 °C for 1 h in presence of He (30 mL/min), the sample was exposed to pure oxygen (30 mL/min) for 30 min, and then cooled to room temperature (RT). After that, the flow was switched to He (30 mL/min) and the reactor was purged for an additional 1 h in order to stabilize the mass spectrometer signals. The temperature was then increased from RT to 800 °C using a linear temperature program at 10°/min and held for 30 min.

Temperature-programmed reduction (TPR) experiments were carried out in the same reactors as for O_2-TPD experiments. Samples (ca. 100 mg) were loaded into a U-shaped tube and heated from room temperature to 800 C (10 °C/min), using a reducing gas mixture of 1 v/v % H_2/He (30 mL/min). H_2 uptake was measured by following the $m/z = 2$ signal with the same mass spectrometer than used for O_2-TPD measurements.

X-ray photoelectron spectroscopy (XPS) spectra were recorded on a KRATOS AXIS Ultra DLD spectrometer using monochromated Al Ka X-ray source (1486.6 eV–140 W) and a pass energy of 20 eV. Charge neutralization was required for all samples. Shirley background subtraction and peak fitting with Gaussian–Lorentzian product peak were performed using an XPS processing program (vision 2.2.6 KRATOS). The Binding Energy (BE) scale was corrected using the C1S peak at 284.6 eV as an internal standard. The accuracy of measurement of the binding energy is ± 0.1 eV while that of FWHM is ± 0.05 eV.

2.3. Catalytic activity—soot oxidation reaction

Catalytic performances of the synthesized perovskites were performed by using Temperature-Programmed Oxidation (TPO) tests on powder mixtures as described elsewhere [4]. The model soot (Printex-U) and the respective catalyst powder (soot:catalyst weight ratio of 1:4) were mixed and crushed for 15 min in a mortar to improve the soot/catalyst agglomerate contact (tight contact mode). Although loose contact condition is closer to real conditions, tight contact condition is helpful to reflect the intrinsic characteristics of the catalysts and more reproducible. TPO analyses were carried out in the presence of 1% O_2 in He (100 mL/min) with a heating ramp of 10°/min from room temperature to 750 °C, on a fixed-bed tubular quartz reactor (internal diameter = 8 mm). The reaction products (CO and CO_2) were continuously recorded with an on-line IR analyzer (EMERSON NGA2000).

3. Results and discussion

3.1. Chemical and structural properties

The chemical compositions deduced from ICP-OES measurements for LaSrxAgFe and LaSrxAgMn perovskites are shown in Table 1. ICP analysis confirm the presence of targeted chemical compositions as well as the expected amount of Ag in the samples. The empirical chemical formula shown in Table 1 reflect the real atomic ratios obtained by the chemical analysis. Nevertheless, it does not necessary correspond to the stoichiometry of the materials considering the unknown state and location of Ag in the perovskite structure.

The XRD patterns obtained for the LaSrxAgMn and LaSrxAgFe perovskite series are presented in Fig. 1a and b, respectively. All the synthesized materials show the feature reflections of the perovskite structure independently of the silver loading with a rhombohedral and an orthorhombic symmetry for manganites and ferrites, respectively. Recently, we have reported [4] that the structure of $La_{0.6}Sr_{04}MnO_3$ and $La_{0.6}Sr_{0.4}FeO_3$ perovskite-type materials, synthesized with the same experimental procedure, is similar. This indicates that the addition of silver does not modify the structure of the perovskites, as expected by

Table 1
Chemical composition and crystal domains of prepared perovskites.

Code	Chemical formula	CS Perovs. (nm)[a]	CS Ag^0 (nm)[b]
LaSrFe	$La_{0.60}Sr_{0.38}FeO_{3-\delta}$	18	–
LaSr5AgFe	$La_{0.51}Sr_{0.46}Ag_{0.05}FeO_{3-\delta}$	17	78
LaSr10AgFe	$La_{0.53}Sr_{0.41}Ag_{0.10}FeO_{3-\delta}$	20	120
LaSr15AgFe	$La_{0.53}Sr_{0.36}Ag_{0.15}FeO_{3-\delta}$	17	125
LaSr20AgFe	$La_{0.53}Sr_{0.31}Ag_{0.20}FeO_{3-\delta}$	26	83
LaSr25AgFe	$La_{0.52}Sr_{0.26}Ag_{0.25}FeO_{3-\delta}$	29	82
LaSrMn	$La_{0.59}Sr_{0.37}MnO_{3-\delta}$	23	–
LaSr5AgMn	$La_{0.54}Sr_{0.49}Ag_{0.05}MnO_{3-\delta}$	20	48
LaSr10AgMn	$La_{0.52}Sr_{0.41}Ag_{0.10}MnO_{3-\delta}$	20	66
LaSr15AgMn	$La_{0.53}Sr_{0.36}Ag_{0.15}MnO_{3-\delta}$	20	45
LaSr20AgMn	$La_{0.54}Sr_{0.32}Ag_{0.20}MnO_{3-\delta}$	21	58
LaSr25AgMn	$La_{0.50}Sr_{0.24}Ag_{0.26}MnO_{3-\delta}$	21	74

[a] Cristal domain size of the perovskite-structure, calculated from its (0 2 4) diffraction peak.
[b] Cristal domain size of Ag^0, calculated from its (1 1 1) diffraction peak.

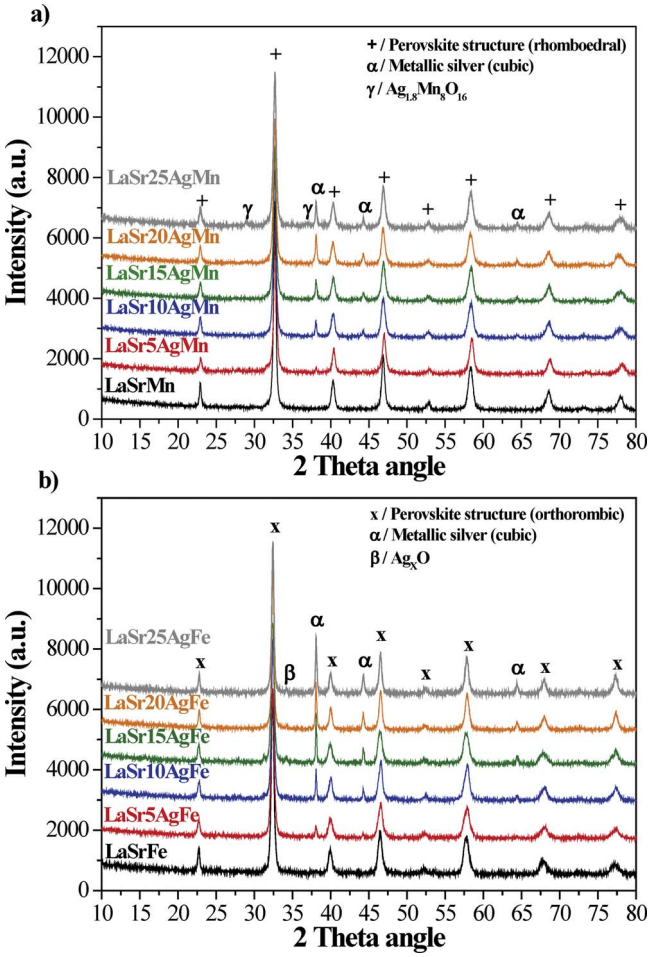

Fig. 1. XRD patterns of synthesized perovskites.

the similarity of the ionic radius of La^{3+} (1.36 Å) and Ag^+ (1.28 Å) cations [28]. The crystallinity of the materials was also unaffected by the presence of silver, maintaining a similar crystal domain size in all the synthesized perovskites (Table 1). On the other hand, additional XRD patterns at 38.1°, 44.3° and 64.4° (2θ°) corresponding to (1 1 1), (2 0 0) and (2 2 0) planes of fcc metallic silver prove the presence of surface metallic Ag. In the case of LaSr25AgMn, small reflections attributed to the presence of $Ag_{1.8}Mn_8O_{16}$ were also identified (2θ° = 29° and 37°). These results show the limited solubility of Ag in the parental perovskite-structure in agreement with the thermodynamic stability of Ag^{00} species above 150 °C in air [29]. It has been very difficult to ascertain the presence of Ag_2O on manganites because the main peaks of Ag_2O (1 1 1) (2θ = 33°) and those of the perovskite structure overlap. In addition, main diffraction peaks of Ag^{00} and Ag_2O are also very close each other, making almost impossible the identification of silver-oxide species [30]. The presence of one small diffraction peak at 34.2°, related to the existence of oxidized silver species (JCPDS-76-1393), has only been evidenced on ferrites except for LaSr5AgFe. Such diffraction peak was not evidenced on manganites except on LaSr25AgMn.

The crystal domain size of metallic silver was estimated from the (1 1 1) diffraction peak (above 38.1° 2θ) by using the Scherrer equation (Table 1). Considering that the (2 0 0) reflection of Ag_2O phase can be overlapped with the (1 1 1) one of metallic silver, calculated values can be over-estimated. Nevertheless, it is clear that the Ag° crystal size is larger on ferrites. For instance, for 10 mol% Ag (LaSr10AgFe and LaSr10AgMn), the crystal domain size of Ag° is approximately two times larger on ferrite (120 nm) than on manganite (66 nm).

3.2. Textural and morphological properties

Figs. 2 and 3 show representative SEM images of perovskites. Their morphology is mainly affected by the nature of the B cation (Fe or Mn), as previously reported [3]. Ferrites (Fig. 2) are mostly characterised by dense foil-shape particles (except LaSr25AgFe material), while manganese-perovskites exhibit a macroporous texture. The LaSr25AgFe morphology is different from other ferrites, showing smaller and granulated particles.

SSA and porosity properties of the synthesized perovskites were analyzed by N_2 adsorption at 77 K (Table 2). The addition of silver does not significantly affect the porosity. Manganites present at least twice bigger SSA and pore volumes than ferrites. However, both types of perovskites keep a similar double distribution of pores with an average pore size in the 14–23 nm range. This means that aggregates of particles forming slit shaped pores mainly generate such porosity. This feature is also reflected in the type-hysteresis loop (H3 or H4) [31] of the physisorption isotherms (Supporting files Figs. S1–S4).

TEM micrographs of LaSr25AgFe and LaSr25AgMn catalysts (Figs. 4 and 5) show aggregates of perovskites crystallites (Figs. 4a and 5a). Some LaSr25AgFe grains have the form of rods (Fig. 4c). TEM images evidence the presence of surface spherical NPs on both perovskites which were identified as silver by EDX analysis (Figs. 4 and 5). This underlines that the dissolution of silver in the perovskite matrix did not take place in a great extent, in agreement with XRD data. However, it can be seen by EDX analysis performed on a LaSr25AgFe grain that some silver might be successfully integrated into the structure (Fig. 4d). Similar analysis were impossible to obtain on LaSr25AgMn. This indicates a slightly better solubility of silver in the ferrite structure.

We have estimated the Ag NPs size distribution on LaSr25AgFe and LaSr25AgMn. LaSr25AgFe shows a wide distribution of particles between 15 and 68 nm, centering at 40 nm, whereas LaSr25AgMn exhibits a narrower range between 9 and 38 nm, centering at 18 nm (Figs. S5 and S6). These results differ quantitatively with those obtained by XRD. As already mentioned, Ag crystal domain size is overestimated. Nevertheless, the trend fits well with XRD estimations, being the particle size smaller for the LaSrxAgMn series. The higher dispersion of Ag NPs on the surface of manganites could also be explained by its higher SSA.

3.3. O_2-TPD analysis

Two different types of oxygen are known in the literature to desorb from perovskites: α-oxygen (suprafacial) and β oxygen (intrafacial) species [32–34]. The temperature range characteristic of the α oxygen can be divided in two sub-regions: below 400 °C, which corresponds to weakly chemisorbed oxygen upon surface-oxygen vacancies, and

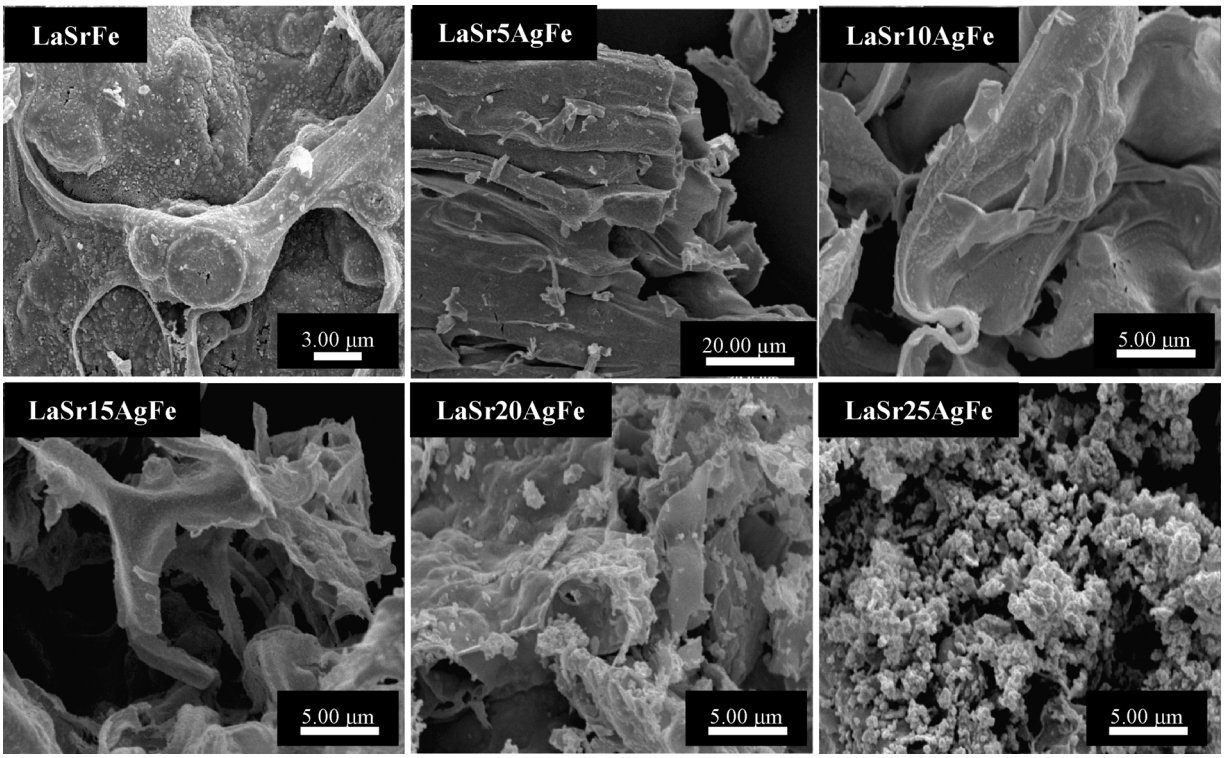

Fig. 2. SEM images of silver containing ferrites (LaSrxAgFe).

between 400 to 700 °C (denoted as α'), ascribed to near-surface oxygen associated to lattice defects such as dislocations and grain frontiers. The β oxygen usually belongs to the oxide bulk [35].

Profiles of O_2-TPD spectra (Fig. 6) clearly depend on the chemical nature of the B-site cation and on the Ag loading. The amount of desorbed oxygen strongly increases with the Ag amount in the manganites (Fig. 6a), starting from 66 µmoles O_2/g_{cat} in LaSrMn to 284 µmoles O_2/g_{cat} in LaSr25AgMn (Table 3). This trend is also valid below 400 °C, where weakly α surface chemisorbed oxygen species are involved, despite similar SSA for all manganites (around 20 m^2/g, Table 2). Similar behaviors have been reported in the literature for $La_{1-x}Ag_xMn_{0.9}Co_{0.1}O_3$ [16] and $Ag/PrMnO_{3+\delta}$ [13] and attributed to the decomposition of surface silver oxide to silver metal. Below 500 °C, spectra of all Ag-modified manganites are very similar, suggesting that the dispersion of

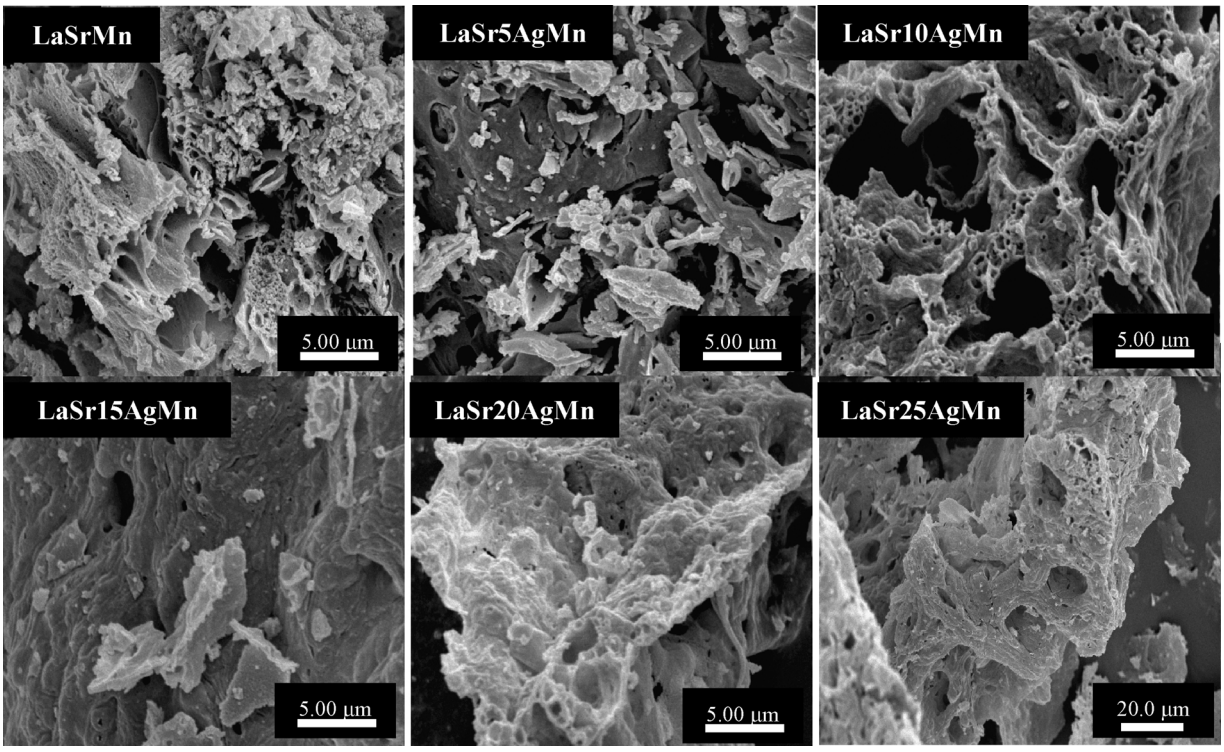

Fig. 3. SEM images of silver containing manganites (LaSrxAgMn).

Table 2
Specific BET area, pore volume and pore size of silver containing ferrites (LaSrxAgFe) and manganites (LaSrxAgMn).

Code	SSA (m^2/g)	V_p (cm^3/g)	Pore size (nm)
LaSrFe	11	0.046	15
LaSr5AgFe	8	0.045	21
LaSr10AgFe	7	0.038	19
LaSr15AgFe	7	0.039	23
LaSr20AgFe	7	0.032	16
LaSr25AgFe	8	0.040	18
LaSrMn	16	0.057	14
LaSr5AgMn	21	0.091	17
LaSr10AgMn	15	0.063	16
LaSr15AgMn	22	0.097	16
LaSr20AgMn	18	0.091	18
LaSr25AgMn	25	0.134	20

surface silver oxide is comparable. This result also confirms the limited solubility of Ag in the manganite structure, as assumed from XRD and TEM. The low amount of oxygen desorbed from LaSrMn in the α and α' temperature regions was ascribed to the presence of a charge compensation mechanism based on the oxidation of Mn^{3+} into Mn^{4+} rather than one based on the generation of surface oxygen vacancies as shown in a previous study [3]. In the temperature region from 400 to 700 °C (α' in Fig. 6a), a strong and well-defined O_2-desorption peak appears above 600 °C on Ag-modified manganites. The intensity and position of this peak vary with the silver content, resulting in more intense peaks on LaSr20AgMn and LaSr25AgMn perovskites, and a shift to higher temperature values (from 570 to 621 °C on LaSr5AgMn and LaSr25AgMn, respectively). Wang et al. [36] reported a very similar O_2-TPD profile for a silver catalyst supported on MnO_x. The strong and sharp oxygen evolution peak at 665 °C was attributed to the formation of $Ag_2Mn_8O_{16}$ phase, in which the electron transfer between Mn^{3+} and Mn^{4+} species favors the desorption of a large amount of oxygen species. This phase $Ag_{1.8}Mn_8O_{16}$ (hollandite-type structure) was clearly identified by XRD in the LaSr25AgMn solid (Fig. 1a). Thus, the oxygen evolution peak observed around 600 °C is probably due to the formation of this phase on the surface, especially on LaSr20AgMn and LaSr25AgMn.

The O_2-TPD spectra of LaSrxAgFe solids are very different compared to those of LaSrxAgMn (Fig. 6b). As previously reported [3], the oxygen desorption from ferrites mainly comes from α and α' temperature regions. This fact was related to the high concentration of surface oxygen vacancies generated in this type of materials as a mechanism of charge compensation due to the partial replacement of La^{3+} by Sr^{2+}. The addition of Ag does not significantly modify the TPD profiles (Fig. 6b)

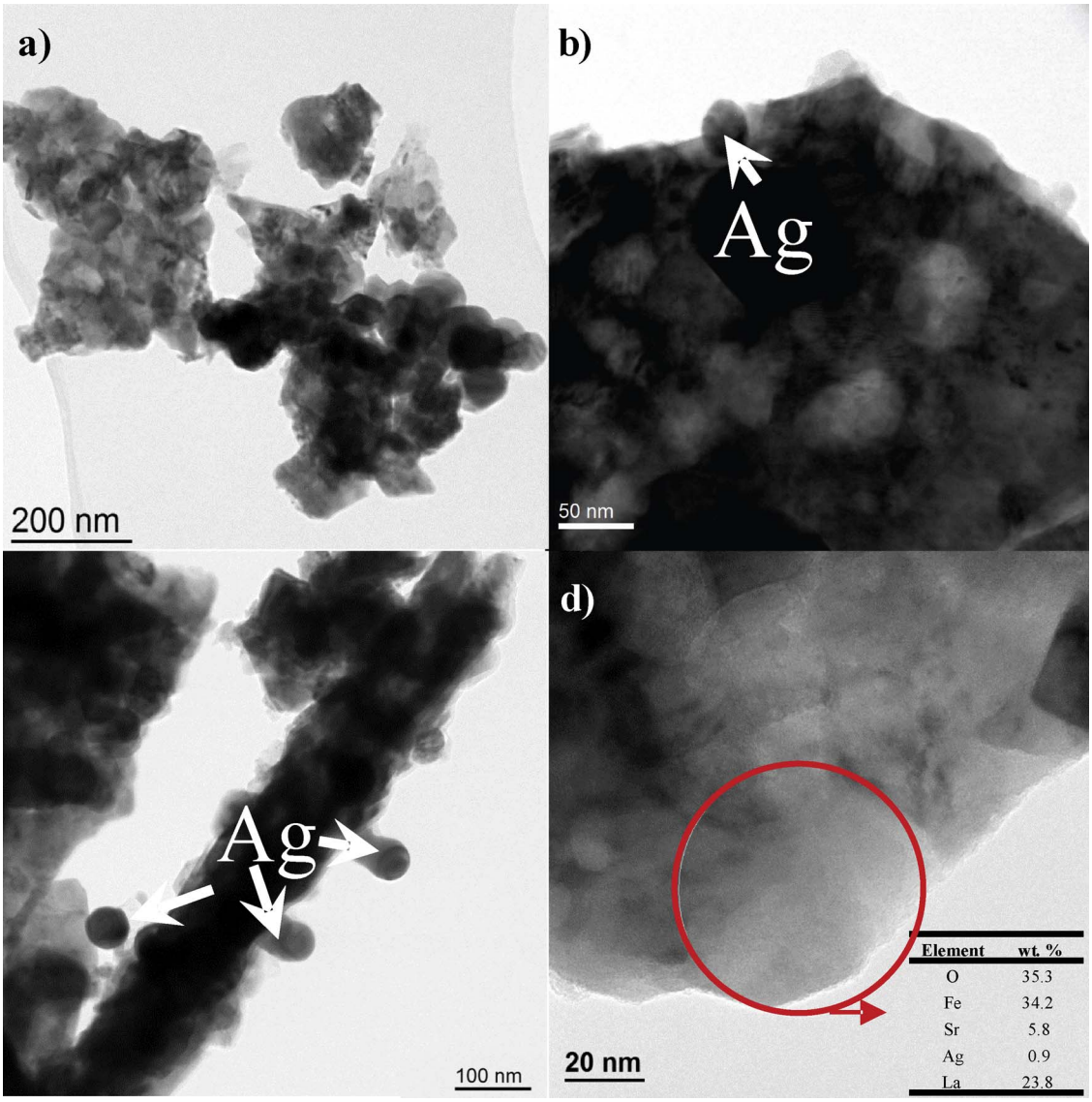

Fig. 4. TEM images of LaSr25AgFe perovskite.

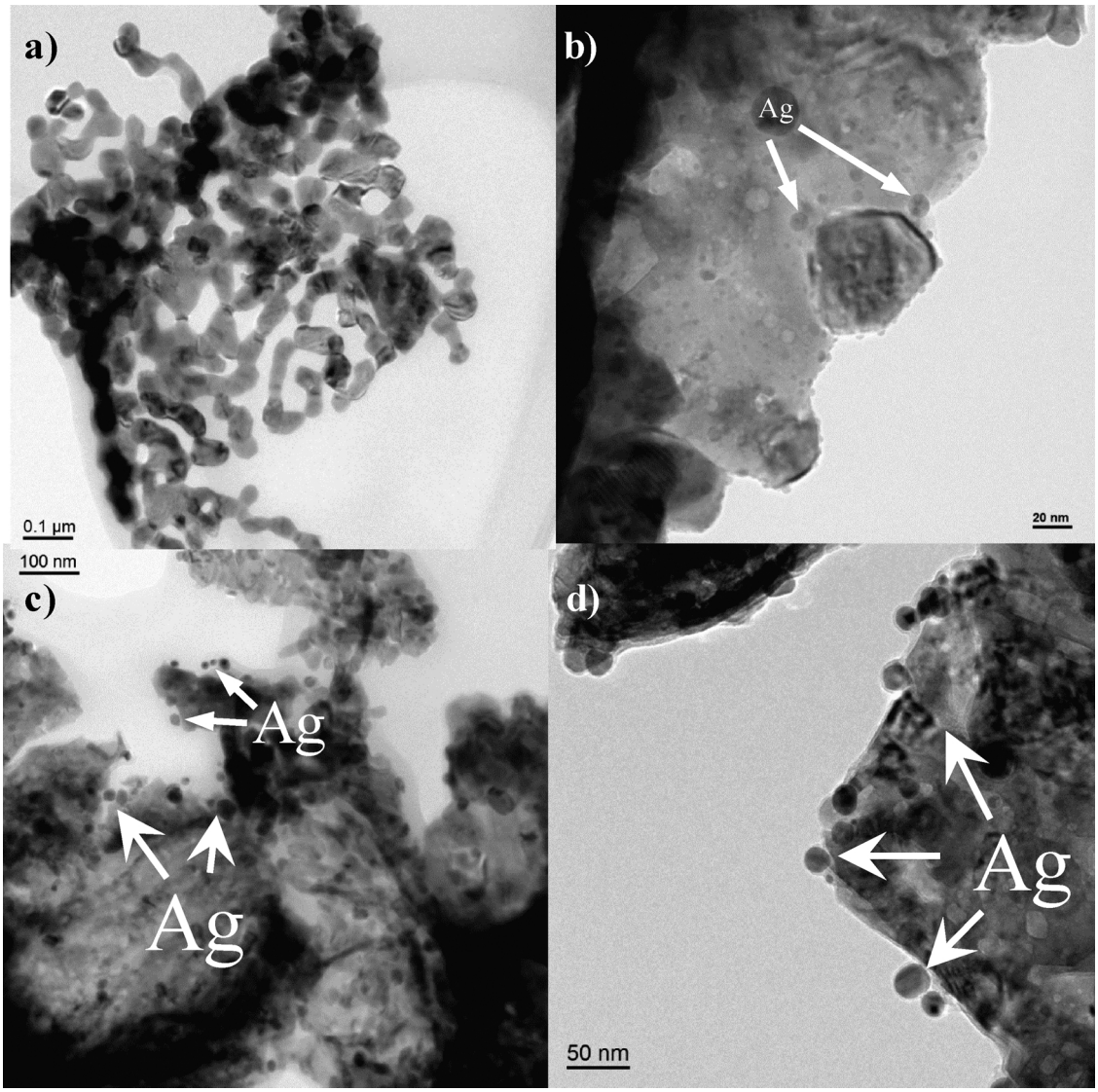

Fig. 5. TEM images of LaSr25AgMn perovskite.

except those of LaSr20AgFe and LaSr25AgFe that show a remarkable decrease in the amount of desorbed O_2 in the α region, while the oxygen coming from the α' one is shifted towards the marked β temperature zone. In addition, only LaSr5AgFe and LaSr10AgFe materials present a larger amount of oxygen released compared to LaSrFe (Table 3). For high Ag contents (LaSr15AgFe, LaSr20AgFe and LaSr25AgFe), the presence of silver is detrimental for the oxygen release capacity, in opposition to the behavior observed on manganites. As above described, the oxygen release capacity of these types of materials is mainly related to the presence of surface oxygen vacancies. These point defects act as anchor places for the stabilization-exchange of oxygen species on the surface. The agglomerated Ag NPs observed by XRD (crystal domain sizes higher than 80 nm, Table 1) and TEM could partially cover these surface oxygen vacancies and block their ability to adsorb and stabilize O_2 from the gas phase. This inhibiting effect was not evidenced on LaSr5AgFe and LaSr10AgFe and even more, an improvement of their oxygen release capacity was observed (Table 3) especially for LaSr5AgFe.

3.4. H_2-TPR analysis

Temperature-programmed reduction (TPR) was performed to assess the reducibility of Ag-substituted perovskites. Fig. 7 shows the TPR profiles of LaSrxAgMn and LaSrxAgFe samples. According to previous studies, the H_2 consumption peaks at low temperature centered at 387 and 492 °C on LaSrMn are related to the desorption of oxygen species from surface oxygen vacancies as well as of lattice oxygen due to the partial reduction of Mn^{4+} to Mn^{3+} [3], respectively. The H_2 consumption at high temperature (i.e. > 650 °C) is linked to the final reduction of Mn^{3+} to Mn^{2+} which leads to the breakdown of the perovskite phase [37].

The introduction of silver in the perovskite structure strongly modifies TPR profiles of manganites below 650 °C. The H_2 consumption increases (Table 4), from 925 µmoles/gcat to 1431 µmoles/gcat for LaSrMn and LaSr25AgMn, respectively. In addition, it is shifted towards lower temperatures. However, this temperature shift and the H_2 consumption are not proportional to the Ag loading in the perovskite. Shoulders at around 100 °C on the TPR spectra can be ascribed to the reduction of surface AgO NPs as already reported on $Ag/PrMnO_3$ [13]. The reduction of Ag_2O to metallic Ag promotes the reduction of the perovskite due to spillover effect [13] of metallic Ag NPs. This explains the shift to lower temperatures of the Mn^{4+} reduction to Mn^{3+}. The H_2 consumption below 200 °C, linked to AgO reduction, is rather small for all manganites except for LaSr15AgMn.

The reducibility of the $Ag_{1.8}Mn_8O_{16}$ phase could also increase the H_2 consumption. It is therefore difficult to clearly explain differences

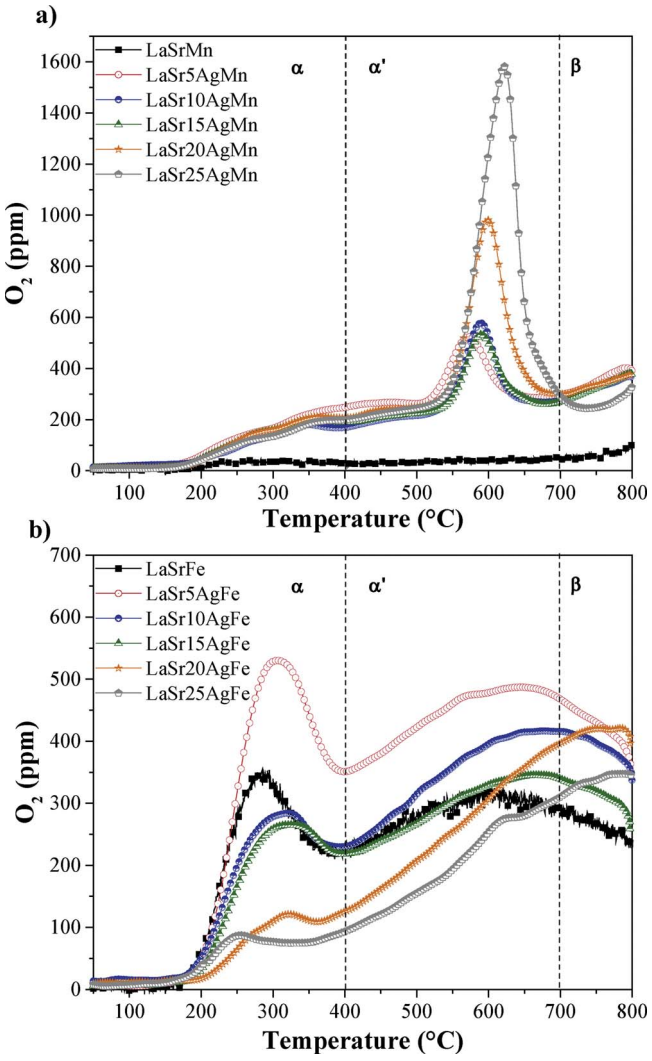

Fig. 6. O_2-TPD profiles of the synthesized: a) LaSrxAgMn and b) LaSrxAgFe materials.

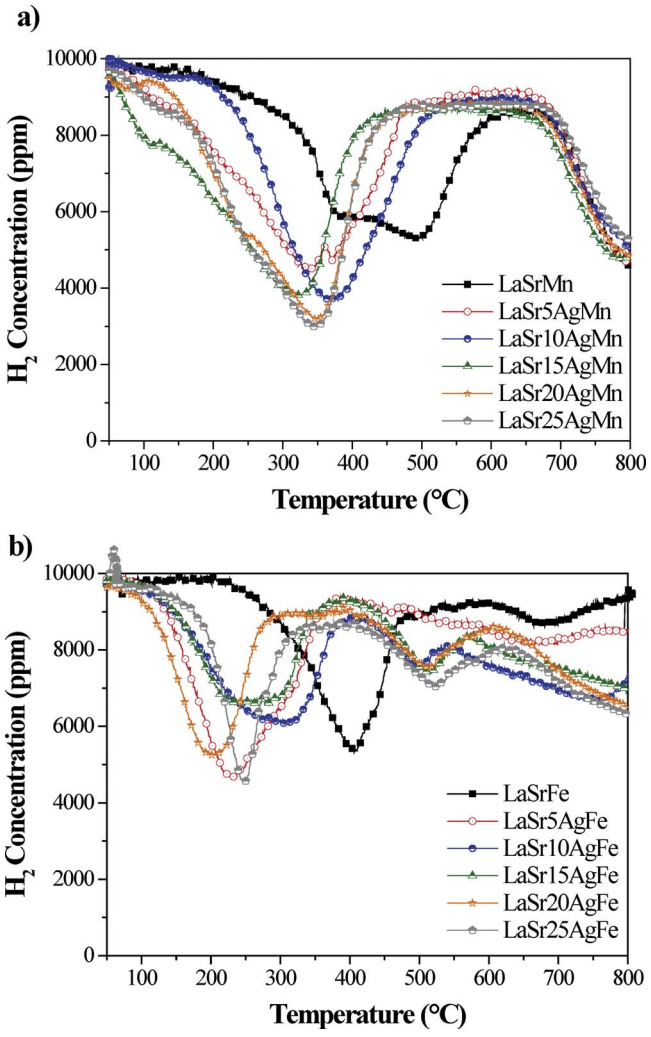

Fig. 7. H_2-TPR profiles of the synthesized: a) LaSrxAgMn and b) LaSrxAgFe materials.

Table 3
Oxygen desorption from LaSrxAgFe and LaSrxAgMn perovskites measured from TPD runs.

Code	O_2 desorbed (μmol/g)
LaSrFe	230
LaSr5AgFe	326
LaSr10AgFe	266
LaSr15AgFe	216
LaSr20AgFe	210
LaSr25AgFe	169
LaSrMn	66
LaSr5AgMn	239
LaSr10AgMn	218
LaSr15AgMn	213
LaSr20AgMn	259
LaSr25AgMn	284

Table 4
H_2 uptake during the first reduction stage of LaSrxAgMn and LaSrxAgFe in the temperature range 100–600 °C and 100–400 °C, respectively.

LaSrFe	596
LaSr5AgFe	808
LaSr10AgFe	557
LaSr15AgFe	541
LaSr20AgFe	520
LaSr25AgFe	394
LaSrMn	925
LaSr5AgMn	1292
LaSr10AgMn	1188
LaSr15AgMn	1345
LaSr20AgMn	1280
LaSr25AgMn	1431

observed between TPR spectra below 650 °C of the various Ag-doped manganites. Nevertheless, one can assume that LaSr15AgMn contains the highest loading of AgO NPs on the surface while LaSr20AgMn and LaSr25AgMn exhibit very similar profiles with the largest H_2 consumption. TPR experiments of manganites also show that the addition of Ag does not modify the bulk reducibility of the perovskites above 650 °C, confirming the low level of incorporation of Ag into the structure. This also indicates that Ag^+ cations inserted in the perovskite structure are not reducible in the studied temperature range.

The TPR spectrum of LaSrFe presents two peaks at 404 and 688 °C. According to literature, the reduction of Fe^{4+} material into Fe^{3+} in LaSrFe would occur at T < 300 °C [3]. Thus, this process could be overlapped by the hydrogen consumption related to the surface oxygen species. The shoulder at 450 °C and the small reduction peak at 690 °C can be ascribed to the reduction of surface Fe^{3+} to Fe^{2+} and to the partial reduction of Fe^{2+} to metallic iron, respectively. The two peaks are shifted to lower temperatures with the Ag addition, most probably

Table 5
Surface features of LaSrFe, LaSrAg25Fe, LaSrMn and LaSrAg25Mn perovskites determined by XPS.

	$Sr3d_{5/2}$		O1s		$Ag3d_{5/2}$	
Catalyst	B.E. (eV)	% Relative content[a]	B.E. (eV)	% Relative content	B.E. (eV)	% Relative content[a]
	131.9	63.7	528.5	51.9	–	–
LaSrFe	133.1	36.3	529.6	16.5		
			530.9	27.3		
			532.3	4.2		
	130.7	10.6	527.2	6.9	367.3	22.5
LaSr25AgFe	132	66.8	528.4	34.8		
	133.2	22.6	529.4	30.5	368.3	77.5
			531	28.3		
	132	76.33	528.9	48	–	–
LaSrMn	133.2	23.67	529.6	21.1		
			531	28.1		
			533.5	2.8		
	132.2	84.7	529.2	54.2	368.1	100
LaSr25AgMn	133.4	15.3	529.9	21.6		
			531.1	21.5		
			533.3	2.7		

[a] Based on the signal of both the $3d_{5/2}$ and $3d_{3/2}$.

due to the H_2 spillover on metallic Ag. As for manganites, surface AgO NPs are reduced to metallic Ag below 200 °C but the H_2 consumption is greater, indicating that the surface concentration of AgO NPs is much higher on ferrites than on manganites.

Except for LaSr5AgFe, the overall H_2 consumption (Table 4) remains similar and even decreases when increasing the silver loading as observed for O_2-TPD profiles. The presence of large Ag particles on the surface, as shown by XRD and TEM, coupled with a low SSA, may limit the reducibility of the perovskites [11]. On the other hand, contrary to manganites, the reducibility above 600 °C increases with the Ag loading. It could be explained by the interaction of lattice Ag^+ cations with iron, making them more easily reduced. Similar effects have been observed with Cu in LaSrFe perovskites by Zhang et al. [38]. These results suggest a lower stability of the Fe^{3+} cation in the perovskite structure when La is partially substituted by Ag^+. This is in line with O_2-TPD, where the bulk-oxygen mobility seemed to be favored at high silver loadings (LaSr20AgFe and LaSr25AgFe).

3.5. XPS analysis

XPS examinations of LaSrMn, LaSr25AgMn, LaSrFe and LaSr25AgFe catalysts were carried out in order to assess the change in the composition of their surfaces by the addition of Ag in the perovskite structure. Table 5 summarizes the peak positions and the relative intensities of the Sr3d, O1s and Ag3d XPS peaks as well as the calculated atomic ratios. XPS Figures are shown in the supplementary files (Figs. S7–S11).

The XPS spectra of La for all catalysts are shown in Fig. S1. The La3d XPS peak in all cases exhibits two well resolved spin-orbit components which are further splitted due to multiplet splitting (satellite peaks) that occurs due to the interaction between unpaired electrons in the valence shell and within the core level during the photoemission process. The position of the $La3d_{5/2}$ peak is, in all cases, between 833.4–833.8 eV and with a spin orbit splitting of around 16.6–16.8 eV between $La3d_{5/2}$ and $La3d_{3/2}$ which is characteristic of the La^{3+} state [39]. There is a small shift towards higher BE of around 0.3 eV when introducing Ag in the ferrite structure which is not appreciable in the manganite catalyst. A similar fact was found by Xiao et al. [40] for La and Fe elements in porous $LaFO_3$ perovskites which suggests an increase of the oxidation state or oxidizing capability of the perovskite which is in relationship with a decrease in the BE of O species.

Fig. S2 shows the Sr3d XPS peak for the four catalysts. In all cases two doublets are present at 131.9–132.2 eV and 133.1–133.4 eV ($Sr3d_{5/2}$) attributed to Sr in the bulk and at the outermost surface of the perovskite structure [41,42]. However, when Ag is present in the perovskite structure (LaSr25AgFe), a third peak at 130.7 eV is also present. A peak at similar position has been reported for $SrFeO_{3-\delta}$ and has been attributed to Sr ions surrounded by vacancies in the oxygen-deficient perovskite structure of $SrO_{(1-x)}$ [42]. The presence of that peak seems to be related to the existence of silver oxide on the surface of the iron perovskite, in good agreement with TPR, and might be related to a component at low BEs in the O1s spectra as it will be discussed. This fact might be related with the integration of the silver in the structure of the ferrite perovskite.

Fig. S3 shows the spectra for the Fe2p and Mn2p for LaSrFe, LaSr25AgFe, LaSrMn and LaSr25AgMn catalysts. The analysis of the Mn2p spectra is a rather complicated task because it contains multiplet splitting features (like in the case of La3d) but also shake up features due to excitation of electrons to bound states, a phenomenon that is common in transition metal oxides associated with paramagnetic species. Additionally, as it was reported before, the BE values of the $Mn2p_{3/2}$ core level are very close for Mn^{2+}, Mn^{3+} and Mn^{4+} [43] thus, an accurate quantification can be rather ambiguous. A direct comparison of the recorded spectra is shown in Fig. S3b. The center of the peak is in both cases at 642 eV between the values that are reported for Mn (III) and Mn(IV) [44] implying the existence of manganese atoms in both states. No significant differences are detected except a rather small higher peak intensity around 641 eV in the case of the LaSrMn (black spectra) that implies a higher content of Mn(III) compared to the sample with Ag (red spectra).

Fig. S3-a presents the Fe2p XPS peak of the LaSr25AgFe with (red line) and LaSrFe (black line). No changes were found linked to the addition of silver in the perovskite. The center of the Fe2p peak remains at 710 eV ($Fe2p_{3/2}$) which is characteristic for Fe^{3+}, although the relatively large width of the peak does not discard the presence of iron atoms in the 4+ oxidation state [44].

The Ag3d XPS peaks are presented in Fig. S4. The analysis shows that in the case of the LaSr25AgMn perovskite, silver is present only in the metallic state ($Ag3d_{5/2}$ = 368.1 eV) [45]. On the other hand on LaSr25AgFe perovskite, the analysis shows that beyond the peak attributed to metallic atoms, a second component is present at 367.3 eV ($Ag3d_{5/2}$) with a relative intensity of 22.5% that is attributed to silver in oxygenated species. These results are in good agreement with TPR spectra which have evidenced a higher concentration of AgO on ferrites.

The deconvoluted O1s XPS peak for all samples are presented in Fig. S5. In all cases, the components at 528.4–529.2 eV and 529.4–529.6 eV are attributed to the lattice oxygen in the perovskite structure and of surface segregated oxides, respectively. The component at 530.9–531.1 eV is related to surface adsorbed oxygen species (O_{ads}) which are mainly in the form of carbonate species as further supported from the C1s component at around 288.6 eV (not shown here), hydroxyl species or weakly bounded oxygen species such as O_2^- and O^- [46]. The component at high BEs (532.3–533.5 eV) is related to surface adsorbed water molecules [47]. In the case of the LaSrFe sample, the deconvolution reveals the existence of another component at low BEs and more specifically at 527.2 eV which represents only 6% of the O1s signal. Computational studies have attributed oxygen atoms with binding energy in the range between 527 and 528.2 eV to un-reconstructured atomic oxygen on Ag(111) and Ag(110) [48]. Moreover, peaks at similar BEs have been attributed to adsorbed molecular oxygen in $La_{1-x}FeO_{3-\delta}$ perovskites [49]. In this case, it seems that this peak is related to the existence of molecular oxygen on the perovskite structure and is related to the existence of the Sr3d peak at 130.7 eV attributed to Sr ions surrounded by vacancies in the oxygen-deficient perovskite structure which could be generated by a certain assimilation of Ag ion in the ferrite structure. Further studies are necessary to have a better insight in this phenomenon.

Table 6
Catalytic performances towards soot conversion for LaSrxAgMn and LaSrxAgFe samples.

	$T_{5\%}$ (°C)	$T_{20\%}$ (°C)	$T_{50\%}$ (°C)	$T_{90\%}$ (°C)	T_m (°C)		S_{CO2}
					LT (°C)	*HT* (°C)	
LaSrFe	426	483	534	586	–	563	99.5
LaSr5AgFe	403	459	511	570	–	529	99.3
LaSr10AgFe	420	477	520	564	–	535	99.4
LaSr15AgFe	423	477	523	567	–	545	99.9
LaSr20AgFe	393	456	510	562	–	527	99.9
LaSr25AgFe	393	456	509	562	–	536	98.8
LaSrMn	428	490	538	593	–	559	99.8
LaSr5AgMn	389	459	508	566	448	527	99.9
LaSr10AgMn	388	457	514	564	432	526	99.9
LaSr15AMn	369	425	487	550	417	512	99.9
LaSr20AgMn	374	429	490	552	417	510	99.9
LaSr25AgMn	367	401	449	543	418	525	99.9

3.6. Soot oxidation reaction

The catalytic performance of the synthesized materials was evaluated for the soot combustion reaction. A low concentration of oxygen in the gas phase (1% v/v), to mimic exhausts of GDI engines, was used. The activity of the catalyst was quantified by different parameters: the temperature at 5% and 50% of soot conversion ($T_{5\%}$ and $T_{50\%}$), the temperature corresponding to the maximum CO_2 concentration (T_m) and the selectivity to CO_2 formation at T_m (S_{CO2}) (Table 6). Fig. 8 shows the light-off curves for the un-catalyzed soot model Printex U, LaSrxAgMn and LaSrxAgFe catalysts as well as the CO_2 and CO production during the oxidation process. It can be seen that in all cases, the presence of a catalyst significantly shifts the soot oxidation process towards lower temperatures. The similar catalytic activity of the bare oxides (LaSrFe and LaSrMn) was attributed to the participation of oxygen species coming from the surface, sub-surface and bulk of the catalyst [3]. The catalytic activity of LaSrFe was ascribed to its ability to adsorb and dissociate oxygen from the gas-phase on surface oxygen vacancies (suprafacial oxygen species), which is later transferred to the soot. On the other hand, the mechanism of soot oxidation in contact with LaSrMn was attributed to the easier reduction of Mn^{4+} to Mn^{3+}. These different mechanisms are derived from the different charge

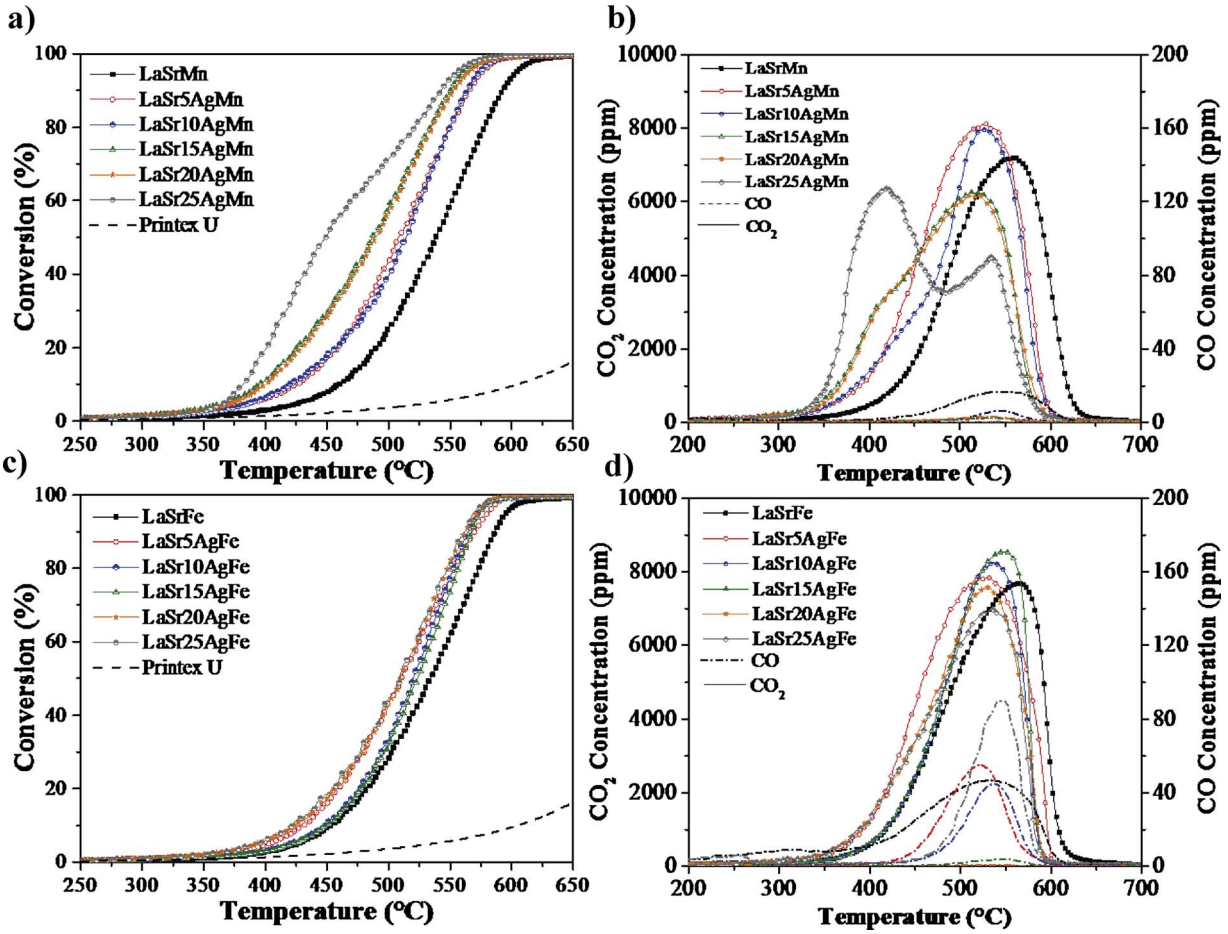

Fig. 8. Soot conversion performances a) light-off curves for LaSrxAgMn catalysts and un-catalyzed Printex U soot model; b) CO_2 (solid line) and CO (dotted line) for LaSrxAgMn catalysts; c) light-off curves for LaSrxAgFe catalysts and un-catalyzed Printex U soot model and d) CO_2 (solid line) and CO (dotted line) for LaSrxAgFe catalysts.

compensation mechanisms between manganites and ferrites as proved in a recent work [3] and confirmed by these O_2-TPD and TPR experiments.

The addition of silver clearly improves the catalytic performances of the synthesized perovskites. Nevertheless, such improvement is much more pronounced for manganites. On ferrites, the enhancement is rather limited, decreasing the $T_{5\%}$ parameter from 426 to 393 °C between LaSrFe and LaSr25AgFe (Table 6). This difference is kept constant in the whole conversion range. In addition, there is not a great impact of the silver loading on the catalytic activity. For instance, $T_{5\%}$ is 403 °C and 393 °C for LaSr5AgFe and LaSr25AgFe, respectively. On the other hand, for the LaSrxAgMn samples, the temperature of the soot ignition was found to be 60 °C lower on LaSr25AgMn than on LaSrMn. In addition, the value of $T_{50\%}$ decreases up to 90 °C. The higher the silver loading, the higher the catalytic activity of manganites.

Despite the low O_2 partial pressure, the production of CO was rather limited for all samples, showing a selectivity towards CO_2 higher than 98% in all cases (Fig. 8b and d). The CO_2 production on ferrites takes place in a single non-symmetrical peak, whereas there is a clear double peak distribution on manganites, which is especially noticeable at the highest Ag loading (LaSr25AgMn). For low Ag loadings (i.e. LaSr5AgMn, LaSr10AgMn), this feature appears as a shoulder rather than a peak. Furthermore, the position of the shoulder and the peak is kept at a similar temperature for all samples, 420 and 520 °C for the low and high temperature peak of CO_2 (denoted as LT and HT on Table 6), respectively.

The location, size and chemical nature of Ag are probably the key parameters that determine the catalytic performances of the different perovskites. Indeed, the soot oxidation capacity of silver-based catalysts has been previously described [13,18–25]. Ag_2O species can act as a strong stoichiometric oxidant for soot combustion, while Ag^0 species promote the formation of active oxygen species such as superoxide ions [19].

For manganites, XRD, TEM, XPS, TPD and TPR analysis have shown that Ag is weakly incorporated into the perovskite structure and is mainly present either as Ag/AgO_x nanoparticles (NPs) or as a surface $Ag_{1.8}Mn_8O_{16}$ additional hollandite-type phase. These two chemical natures of Ag strongly improve the oxygen storage capacity and the reducibility of the manganites, in the low temperature range for AgO_x/Ag NPs and above 500 °C for the hollandite phase. The contribution of the reducible hollandite phase in the amount of oxygen release during TPD in the α' temperature domain is quite significant. The higher the Ag loading, the higher the α' desorption peak. This is consistent with the gradual increase of the catalytic performance of the manganites with the Ag loading.

For ferrites, XRD and TEM analysis have shown that Ag is either partially incorporated into the perovskite structure or present on the surface as nanoparticles. These latter are predominantly in the oxidizing state, i.e. AgO_x, as shown by TPR and XPS. However, except for LaSr5AgFe, the impact of the addition of Ag on TPD and TPR spectra below 600 °C is not beneficial with a decrease of the oxygen release during TPD and no enhancement of the overall H_2 consumption during TPR. This is consistent with the rather limited improvement of the catalytic performances with the addition of Ag. These results can be attributed to the higher solubility of Ag into the structure of ferrites which limits the Ag/soot interactions. This was observed by Megarajan et al. [13], who compared catalytic performances of perovskites with silver species highly dispersed on the surface and silver forming a solid solution. They found that surface dispersed Ag NPs show a better catalytic activity than the Ag substituted counterpart. Furthermore, TEM and XRD have evidenced a greater agglomeration of Ag NPs on ferrites than on manganites leading to large Ag particles on ferrites. For high Ag loadings, these big Ag agglomerates can partially cover the perovskite surface including the oxygen vacancies. This decoration of the surface by Ag can inhibit the ability of oxygen vacancies to adsorb and stabilize O_2 from the gas phase, then lowering the catalytic activity for soot combustion. Indeed, oxygen species weakly adsorbed on surface oxygen vacancies have been proposed to be responsible for soot combustion between 300 and 500 °C [50].

The better catalytic performance of manganites in comparison to ferrites could also be partially explained by a more intimate contact [51–54] between the catalyst surface and the soot particles due to the open macropores observed on manganites (Fig. 3). The open macropores, in the size range 0.2–15 µm, are bigger than soot grapes, suggesting that these latter can enter into the pores of manganites, then increasing the Ag/soot interactions.

The hydrothermal activity of the best catalyst, i.e. LaSr25AgMn was also evaluated as a large quantity of steam is present in GDI exhausts. The addition of 10% vol. of H_2O in the gas stream does not hinder but slightly improves the catalytic performances of the manganite (Fig. S12). This underlines the good catalytic properties of this material. This promoting effect could be due to the formation of OH groups that may facilitate the re-oxidation of oxygen vacancies and thus, enhancing the soot oxidation reaction.

The comparison of the catalytic results of this study with literature data is tricky since the soot oxidation rate depends on many parameters such as the soot/catalyst ratio, the pretreatment of the catalyst, the type of soot, the quality of the soot/catalyst contact, the oxygen concentration… Nevertheless, we have retorted in Table S1 values of the temperatures corresponding to the maximum CO_2 concentration (Tm) achieved in similar conditions for different catalytic materials. Performances of LaSr25AgMn in presence of 1% O_2 are similar with those of a fresh Ag/CeO_2 catalyst [55] (5 wt.% Ag, calcined at 500 °C for 3 h), whereas LaSr25AgMn was calcined at much higher temperature, i.e. 800 °C for 4 h. Furthermore, the Tm value of LaSr25AgMn is slightly lower than that of $La_{0.8}K_{0.20}MnO_3$ [56] (calcined at 800 °C) which was tested in the presence of NO, which is known to promote the soot oxidation rate via the production of NO_2. This comparison with literature data confirms the promising catalytic performances for GDI soot oxidation of LaSr25AgMn.

4. Conclusions

This study reports, for the first time, catalytic performances of Ag-modified manganite (LaSrxAgMn) and ferrite (LaSrxAgFe) perovskites towards soot oxidation under gasoline direct injection engines conditions, i.e. low O_2 partial pressure. Perovskites were synthesized by a complex route and calcined at 800 °C. The state and location of silver determine the catalytic performances of perovskites. On LaSrxAgFe, Ag is either partially incorporated on the ferrite structure or present on the surface as large agglomerates. Ag^+ cations in the structure are not catalytically active for the reaction. Furthermore, large surface Ag particles partially cover surface oxygen vacancies and block their ability to adsorb oxygen. On the other hand, on LaSrxAgMn catalysts, Ag is mainly present either as surface Ag/AgO_x nanoparticles or as a surface $Ag_{1.8}Mn_8O_{16}$ additional hollandite-type phase. These two chemical natures of Ag improve the reducibility and the oxygen storage capacity of the perovskite, acting as catalytically active sites for soot oxidation. This promoting effect of Ag coupled with a suitable macroporous morphology make Ag-modified manganites a promising material for catalyzed gasoline particulate filters.

Acknowledgements

This study was performed in the "Triptic-H" project, partially funded by the French National Research Agency (ANR), ANR-2011-VPTT-003.

Appendix A. Supplementary data

Supplementary data associated with this article can be found, in the online version, at https://doi.org/10.1016/j.apcatb.2017.12.029.

References

[1] A. Mamakos, N. Steininger, G. Martini, P. Dilara, Y. Drossinos, Cost effectiveness of particulate filter installation on direct injection gasoline vehicles, Atmos. Environ. 77 (2013) 16–23.

[2] D. Lopez-Gonzalez, M. Tsampas, A. Boréave, L. Retailleau-Mevel, M. Klotz, C. Tardivat, B. Cartoixa, K. Pajot, P. Vernoux, Mixed ionic-electronic conducting catalysts for catalysed gasoline particulate filters, Top. Catal. 58 (2015) 1242–1255.

[3] W.Y. Hernández, M.N. Tsampas, C. Zhao, A. Boreave, F. Bosselet, P. Vernoux, La/Sr-based perovskites as soot oxidation catalysts for gasoline particulate filters, Catal. Today 258 (Part 2) (2015) 525–534.

[4] E. Aneggi, C. De Leitenburg, A. Trovarelli, Ceria-based formulations for catalysts for diesel soot combustion, in: A. Trovarelly, P. Fornasierro (Eds.), Catalysis by Ceria and Related Materials, Imperial College Press, London, 2013, pp. 565–621.

[5] M. Piumetti, S. Bensaid, N. Russo, D. Fino, Nanostructured ceria-based catalysts for soot combustion: investigations on the surface sensitivity, Appl. Catal. B 165 (2015) 742–751.

[6] L. Castoldi, R. Matarrese, L. Lietti, P. Forzatti, Intrinsic reactivity of alkaline and alkaline-earth metal oxide catalysts for oxidation of soot, Appl. Catal. B 90 (2009) 278–285.

[7] E. Obeid, M.N. Tsampas, S. Jonet, A. Boréave, L. Burel, M.C. Steil, G. Blanchard, K. Pajot, P. Vernoux, Isothermal catalytic oxidation of diesel soot on Yttria-stabilized zirconia, Solid State Ionics 262 (2014) 253–256.

[8] E. Obeid, L. Lizarraga, M.N. Tsampas, A. Cordier, A. Boréave, M.C. Steil, G. Blanchard, K. Pajot, P. Vernoux, Continuously regenerating diesel particulate filters based on ionically conducting ceramics, J. Catal. 309 (2014) 87–96.

[9] B. Ura, J. Trawczyński, A. Kotarba, W. Bieniasz, M.J. Illán-Gómez, A. Bueno-López, F.E. López-Suárez, Effect of potassium addition on catalytic activity of $SrTiO_3$ catalyst for diesel soot combustion, Appl. Catal. B 101 (2011) 169–175.

[10] M.A. Peña, J.L.G. Fierro, Chemical structures and performance of perovskite oxides, Chem. Rev. 101 (2001) 1981–2018.

[11] P. Ciambelli, S. Cimino, L. Lisi, M. Faticanti, G. Minelli, I. Pettiti, P. Porta, La, Ca and Fe oxide perovskites: preparation, characterization and catalytic properties for methane combustion, Appl. Catal. B 33 (2001) 193–203.

[12] S. Furfori, N. Russo, D. Fino, G. Saracco, V. Specchia, NO SCR reduction by hydrogen generated in line on perovskite-type catalysts for automotive diesel exhaust gas treatment, Chem. Eng. Sci. 65 (2010) 120–127.

[13] S.K. Megarajan, S. Rayalu, M. Nishibori, Y. Teraoka, N. Labhsetwar, Effects of surface and bulk silver on $PrMnO_{3+\delta}$ perovskite for CO and soot oxidation: experimental evidence for the chemical state of silver, ACS Catal. 5 (2015) 301–309.

[14] Z. Liu, Z. Hao, H. Zhang, Y. Zhuang, Study of perovskite-type oxides and their supported Ag derivatives for catalytic oxidation of diesel soot, J. Chem. Technol. Biotechnol. 77 (2002) 800–804.

[15] K. Wang, L. Qian, L. Zhang, H. Liu, Z. Yan, Simultaneous removal of NOx and soot particulates over $La_{0.7}Ag_{0.3}MnO_3$ perovskite oxide catalysts, Catal. Today 158 (2010) 423–426.

[16] R. Dinamarca, X. Garcia, R. Jimenez, J.L.G. Fierro, G. Pecchi, Effect of A-site deficiency in $LaMn_{0.9}Co_{0.1}O_3$ perovskites on their catalytic performance for soot combustion, Mater. Res. Bull. 81 (2016) 134–141.

[17] S. Böcklein, S. Günther, J. Wintterlin, High-pressure scanning tunneling microscopy of a silver surface during catalytic formation of ethylene oxide, Ang. Chem. Int. Ed. 52 (2013) 5518–5521.

[18] E. Aneggi, J. Llorca, C. de Leitenburg, G. Dolcetti, A. Trovarelli, Soot combustion over silver-supported catalysts, Appl. Catal. B 91 (2009) 489–498.

[19] G. Corro, U. Pal, E. Ayala, E. Vidal, Diesel soot oxidation over silver-loaded SiO_2 catalysts, Catal. Today 212 (2013) 63–69.

[20] L. Castoldi, E. Aneggi, R. Matarrese, R. Bonzi, J. Llorca, A. Trovarelli, L. Lietti, Silver-based catalytic materials for the simultaneous removal of soot and NOx, Catal. Today 258 (2015) 405–415.

[21] K. Yamazaki, T. Kayama, F. Dong, H. Shinjoh, A mechanistic study on soot oxidation over CeO_2-Ag catalyst with 'rice-ball' morphology, J. Catal. 282 (2011) 289–298.

[22] K. Yamazaki, Y. Sakakibara, F. Dong, H. Shinjoh, The remote oxidation of soot separated by ash deposits via silver-ceria composite catalysts, Appl. Catal. A 476 (2014) 113–120.

[23] K.I. Shimizu, H. Kawachi, S.I. Komai, K. Yoshida, Y. Sasaki, A. Satsuma, Carbon oxidation with Ag/ceria prepared by self-dispersion of Ag powder into nano-particles, Catal. Today 175 (2011) 93–99.

[24] K.I. Shimizu, H. Kawachi, A. Satsuma, Study of active sites and mechanism for soot oxidation by silver-loaded ceria catalyst, Appl. Catal. B 96 (2010) 169–175.

[25] H. Shimokawa, Y. Kurihara, H. Kusaba, H. Einaga, Y. Teraoka, Comparison of catalytic performance of Ag- and K-based catalysts for diesel soot combustion, Catal. Today 185 (2012) 99–103.

[26] S. Nakayama, $LaFeO_3$ perovskite-type oxide prepared by oxide-mixing, co-precipitation and complex synthesis methods, J. Mater. Sci. 36 (2001) 5643–5648.

[27] V. Roche, A. Hadjar, J.P. Deloume, T. Pagnier, R. Revel, C. Roux, E. Siebert, P. Vernoux, Physicochemical origins of electrochemical promotion of LASRMN/YSZ, Catal. Today 146 (2009) 266–273.

[28] R.D. Shannon, Revised effective ionic radii and systematic studies of interatomic distances in halides and chalcogenides, Acta Crystallographic A 32 (1976) 751–767.

[29] J. Assal, B. Hallstedt, L.J. Gauckler, Thermodynamic assessment of the silver-oxygen system, J. Am. Ceram. Soc. 80 (1997) 3054–3060.

[30] G.R. Khayati, K. Janghorban, The nanostructure evolution of Ag powder synthesized by high energy ball milling, Adv. Powder Technol. 23 (2012) 393–397.

[31] G. Leofanti, M. Padovan, G. Tozzola, B. Venturelli, Surface area and pore texture of catalysts, Catal. Today 41 (1998) 207–219.

[32] J.Y. Zhang, X.L. Weng, Z.B. Wu, Y. Liu, H.Q. Wang, Facile synthesis of highly active $LaCoO_3$/MgO composite perovskite via simultaneous co-precipitation in supercritical water, Appl. Catal. B 126 (2012) 231–238.

[33] M. Dhakad, S.S. Rayalu, R. Kumar, P. Doggali, S. Bakardjieva, J. Subrt, T. Mitsuhashi, H. Haneda, N. Labhsetwar, Low cost, ceria promoted perovskite type catalysts for diesel soot oxidation, Catal. Lett. 121 (2008) 137–143.

[34] R. Pereniguez, J.L. Hueso, F. Gaillard, J.P. Holgado, A. Caballero, Study of oxygen reactivity in $La_{1-x}Sr_{(x)}CoO_{3-delta}$ perovskites for total oxidation of toluene, Catal. Lett. 142 (2012) 408–416.

[35] N.A. Merino, B.P. Barbero, P. Grange, L.E. Cadús, $La_{1-x}Ca_xCoO_3$ perovskite-type oxides: preparation, characterisation, stability, and catalytic potentiality for the total oxidation of propane, J. Catal. 231 (2005) 232–244.

[36] X. Wang, Y.-C. Xie, Characterization of Ag and Ba-modified manganese oxide catalysts: unraveling the factors leading to their enhanced CH_4 oxidation activity, New J. Chem. 25 (2001) 964–969.

[37] D.V. Ivanov, L.G. Pinaeva, L.A. Isupova, A.N. Nadeev, I.P. Prosvirin, L.S. Dovlitova, Insights into the reactivity of $La_{1-x}Sr_xMnO_3$ ($x = 0 \div 0.7$) in high temperature N_2O decomposition, Catal. Lett. 141 (2011) 322–331.

[38] R. Zhang, H. Alamdari, S. Kaliaguine, Fe-based perovskites substituted by copper and palladium for NO + CO reaction, J. Catal. 242 (2006) 241–253.

[39] O.P. Taran, A.B. Ayusheev, O.L. Ogorodnikova, I.P. Prosvirin, L.A. Isupova, V.N. Parmon, Perovskite-like catalysts $LaBO_3$ (B = Cu, Fe Mn, Co, Ni) for wet peroxide oxidation of phenol, Appl. Catal. B 180 (2016) 86–93.

[40] P. Xiao, L. Zhong, J. Zhu, J. Hong, J. Li, H. Li, Y. Zhu, CO and soot oxidation over macroporous perovskite $LaFeO_3$, Catal. Today 258 (2015) 660–667.

[41] P.A.W. Van Der Heide, Systematic x-ray photoelectron spectroscopic study of $La_{1-x}Sr_x$-based perovskite-type oxides, Surf. Interface Anal. 33 (2002) 414–425.

[42] M. Ghaffari, H. Huang, O.K. Tan, M. Shannon, Band gap measurement of $SrFeO_{3-\delta}$ by ultraviolet photoelectron spectroscopy and photovoltage method, Cryst. Eng. Comm. 14 (2012) 7487–7492.

[43] A.J. Nelson, J.G. Reynolds, J.W. Roos, Core-level satellites and outer core-level multiplet splitting in Mn model compounds, J. Vac. Sci. Technol. A 18 (2000) 1072–1076.

[44] M.C. Biesinger, B.P. Payne, A.P. Grosvenor, L.W.M. Lau, A.R. Gerson, R.S.C. Smart, Resolving surface chemical states in XPS analysis of first row transition metals, oxides and hydroxides: Cr, Mn, Fe, Co and Ni, Appl. Surf. Sci. 257 (2011) 2717–2730.

[45] M. Fee, S. Ntais, A. Weck, E.A. Baranova, Electrochemical behavior of silver thin films interfaced with yttria-stabilized zirconia, J. Solid State Electrochem. 18 (2014) 2267–2277.

[46] Z. Gao, H. Wang, H. Ma, Z. Li, Preparation and characterization of the non-stoichiometric La–Mn perovskites, J. Alloys Compd. 646 (2015) 73–79.

[47] H. Arandiyan, H. Dai, J. Deng, Y. Liu, B. Bai, Y. Wang, X. Li, S. Xie, J. Li, Three-dimensionally ordered macroporous $La_{0.6}Sr_{0.4}MnO_3$ with high surface areas: active catalysts for the combustion of methane, J. Catal. 307 (2013) 327–339.

[48] T.E. Jones, T.C.R. Rocha, A. Knop-Gericke, C. Stampfl, R. Schlögl, S. Piccinin, Insights into the electronic structure of the oxygen species active in alkene epoxidation on silver, ACS Catal. 5 (2015) 5846–5850.

[49] J. Faye, A. Baylet, M. Trentesaux, S. Royer, F. Dumeignil, D. Duprez, S. Valange, J.-M. Tatibouët, Influence of lanthanum stoichiometry in $La_{1-x}FeO_{3-\delta}$ perovskites on their structure and catalytic performance in CH_4 total oxidation, Appl. Catal. B 126 (2012) 134–143.

[50] N. Guilhaume, B. Bassou, G. Bergeret, D. Bianchi, F. Bosselet, A. Desmartin-Chomel, B. Jouguet, C. Mirodatos, In situ investigation of diesel soot combustion over an $AgMnO_x$ catalyst, Appl. Catal. B 119–120 (2012) 287–296.

[51] B. Bassou, N. Guilhaume, K. Lombaert, C. Mirodatos, D. Bianchi, Experimental microkinetic approach of the catalytic oxidation of diesel soot by ceria using temperature-programmed experiments. Part 1: impact and evolution of the ceria/soot contacts during soot oxidation, Energy Fuels 24 (2010) 4766–4780.

[52] B. Bassou, N. Guilhaume, K. Lombaert, C. Mirodatos, D. Bianchi, Experimental microkinetic approach of the catalytic oxidation of diesel soot by ceria using temperature-programmed experiments. Part 2: kinetic modeling of the impact of the ceria/soot contacts on the rate of oxidation, Energy Fuels 24 (2010) 4781–4792.

[53] J.P.A. Neeft, M. Makkee, J.A. Moulijn, Catalysts for the oxidation of soot from diesel exhaust gases. I. An exploratory study, Appl. Catal. B 8 (1996) 57–78.

[54] S.B. Simonsen, S. Dahl, E. Johnson, S. Helveg, Ceria-catalyzed soot oxidation studied by environmental transmission electron microscopy, J. Catal. 255 (2008) 1–5.

[55] Y. Gao, A. Duan, S. Liu, X. Wu, W. Liu, M. Li, S. Chen, X. Wang, D. Weng, Study of $Ag/Ce_xNd_{1-x}O_2$ nanocubes as soot oxidation catalysts for gasoline particulate filters: balancing catalyst activity and stability by Nd doping, Appl. Catal. B 203 (2017) 116–126.

[56] H. Wang, J. Liu, Z. Zhao, Y. Weia, C. Xua, Comparative study of nanometric Co-, Mn- and Fe-based perovskite-type complex oxide catalysts for the simultaneous elimination of soot and NOx from diesel engine exhaust, Catal. Today 184 (2012) 288–300.